

Precise Mass Measurement of the ^{108,110,112,114,116}Rh ground state and isomeric state(s)

B. Liu,^{1,2} M. Brodeur,¹ J.A. Clark,² I. Dedes,³ J. Dudek,⁴ F. G. Kondev,² D. Ray,^{5,2} G. Savard,^{2,6} A.A. Valverde,^{5,2} D.P. Burdette,² A.M. Houff,¹ R. Orford,⁷ W.S. Porter,¹ F. Rivero,¹ K.S. Sharma,⁵ and L. Varriano^{6,2,8}

¹*Department of Physics, University of Notre Dame, Notre Dame, IN 46556, USA*

²*Physics Division, Argonne National Laboratory, Lemont, IL 60439, USA*

³*Institute of Nuclear Physics Polish Academy of Sciences, PL-31 342 Kraków, Poland*

⁴*Université de Strasbourg, CNRS, IPHC UMR 7178, F-67 000 Strasbourg, France*

⁵*Department of Physics and Astronomy, University of Manitoba, Winnipeg, MB R3T 2N2, Canada*

⁶*Department of Physics, University of Chicago, Chicago, IL 60637, USA*

⁷*Nuclear Science Division, Lawrence Berkeley National Laboratory, Berkeley, California 94720, USA*

⁸*Center for Experimental Nuclear Physics and Astrophysics, University of Washington, Seattle, WA 98195*

(Dated: October 2, 2024)

Precise mass measurements of the ^{108,110,112,114,116}Rh ground and isomeric states were performed using the Canadian Penning Trap at Argonne National Laboratory, showing a good agreement with recent JYFLTRAP measurements. A new possible isomeric state of ¹¹⁴Rh was also observed. These isotopes are part of the longest odd-odd chain of identical spin-parity assignment, of 1^+ , spanning ^{104–118}Rh, despite being in a region of deformation. Theoretical calculations were performed to explain this phenomenon. In addition, multi-quasiparticle blocking calculations were conducted to study the configuration of low-lying states in the odd-odd Rh nuclei and elucidate the observed anomalous isomeric yield ratio of ¹¹⁴Rh.

PACS numbers: 21.10.Tg, 23.40.-s, 24.80.+y

INTRODUCTION

Nuclear shape is a fundamental property that can provide information on the underlying structure of the nucleus. While doubly magic nuclei are spherical, the shape of nucleus with partially filled shells vary widely across the nuclear chart. The nuclear shape can change not only rapidly from one nucleus to its neighbor but also between the ground state and excited states of the same nucleus where shape coexistence could also happen at similar energies [1].

Certain excited states, called spin-trap isomers, have a large spin difference compared to their ground state, resulting in a suppressed γ transition to the ground state [2]. These isomers, usually strengthened by the complexity of the particle-hole excited structures, are useful to understand single-particle excitation energies and spin-dependent residual interactions between unpaired nucleons, which are essential inputs to study the structure of odd-odd nuclei with deformation. However, the long lifetime of these isomers makes their gamma spectroscopy study challenging. On the other hand, such long lifetimes are ideal for performing an identification and mass measurement of these states using the phase-imaging ion-cyclotron-resonance (PI-ICR) Penning trap mass spectrometry technique [2, 3].

The odd-odd Rh isotopes from ¹⁰⁴Rh to ¹¹⁸Rh are particularly interesting not only because they are mid-shell, in a region of deformation, but also for a few other unique features. Firstly, the spin and parity assignment of the ground state of all these isotopes is 1^+ [4]. Assuming that all assignments are correct, this is the longest chain

of odd-odd isotopes with the same spin and parity in the entirety of the chart of the nuclides. To make it even more unusual, it is in a region of rapid change in nuclear shape (from prolate to oblate), which affects single particle orbitals and usually results in a change in the nuclear spin. Secondly, all of these isotopes have low-lying excited states with very similar excitation energies, where it is slightly lower for ^{110,112}Rh.

In this article, these peculiar aspects of neutron-rich odd-odd Rh isotopes are investigated using a multi-prong approach. Firstly, precision mass measurements of the ^{108,110,112,114,116}Rh ground states and first isomeric states were performed, confirming recent Penning trap measurements [5] while discovering one more isomeric state. Secondly, detailed deformed Woods-Saxon Hamiltonian [6] in its universal parametrization calculations (similar to [7]) of the single particle energy levels of these isotopes were performed resulting in an explanation of the peculiar spin and parity assignment of their ground states. Finally, multi-quasiparticle blocking calculations (similar to [2]) were performed to predict the configuration of low-lying states in the odd-odd Rh nuclei and investigate the anomalous yield of ¹¹⁴Rh.

EXPERIMENT

Experiment Setup

The precise mass measurement of neutron-rich Rh isotopes was conducted using the Canadian Penning Trap (CPT) at the Californium Rare Isotope Breeder Upgrade (CARIBU) facility [8] at Argonne National Laboratory

(ANL). At CARIBU, a ^{252}Cf fission source located at one end of a gas catcher provides a wide range of fission products. The helium filled gas catcher collects these fission products and guides them out with the DC and RF fields applied. After the gas catcher, an isobar separator with a resolving power of $\sim 10,000$ selects the beam based on A/q to remove non-isobaric contaminants [9]. This continuous beam is then cooled and bunched by a radio-frequency quadrupole (RFQ) cooler-buncher. After that, the bunched beam is sent to a multi-reflection time-of-flight mass spectrometer (MR-TOF) to gain further time-of-flight separation between the ion of interest and other isobaric isotope and molecules, with a resolving power of around 100,000 [10]. By controlling the gate time of a Bradbury-Nielsen gate (BNG), the ions of interest are selected and sent to the CPT tower. The CPT tower has a linear trap serving as the preparation trap to cool the ions to minimize energy dispersion before the CPT. A position-sensitive microchannel plate detector (PS-MCP) is located after the CPT to record the ions ejected from the CPT.

Measurement method

In Penning Trap mass spectrometry, the mass of an ion is determined from a measurement of its cyclotron frequency

$$\nu_c = \frac{qB}{2\pi m} \quad (1)$$

where B is the magnetic field, q and m are the charge and mass of the ion. This frequency can be measured using various techniques including the time-of-flight ion-cyclotron-resonance (TOF-ICR) method [11, 12] and the PI-ICR techniques. The latter technique yields higher resolving power and better precision on short-lived isotopes produced at low rate by measuring the phase of the ion clusters to determine the cyclotron frequency. The PI-ICR technique was used for the presented measurements.

The ion motion perpendicular to the axis of a Penning trap is a composition of a reduced cyclotron and a magnetron motion of different frequencies. The sum of the frequency of these motion equals the cyclotron frequency and can be measured directly using the scheme presented in [13]. The ions are first excited by a dipole excitation to a certain radius and rotate with the reduced cyclotron frequency for a given amount of time, called accumulation time t_{acc} . Ions with different mass-to-charge ratios have different reduced cyclotron frequencies and thus acquire different phases during this time period. Then the ions are converted into magnetron motion by the quadrupole excitation before the ions are ejected. For a measurement, a reference spot is first recorded with zero accumulation time and a final spot is measured at

a given non-zero t_{acc} . The total phase difference ϕ_{tot} is determined by the phase difference ϕ_{diff} between the two spots and the additional number of turns N which the final spot acquired. Finally, the cyclotron frequency ν_c can be calculated from the total phase accumulated ϕ_{tot} during t_{acc} using

$$\nu_c = \frac{\phi_{tot}}{2\pi t_{acc}} = \frac{\phi_{diff} + 2\pi N}{2\pi t_{acc}}. \quad (2)$$

With longer t_{acc} , better precision can be achieved. By measuring the cyclotron frequency of two isotopes, the mass ratio of the two isotopes is obtained. Thus the mass of interest can be determined by this ratio together with the mass of the calibration.

Experimental details

To guarantee the accuracy of the measurement and avoid systematic uncertainties from having overlapping clusters of different species, prior to any measurement, great care was taken to identify the isotope of interest as well as all the neighbouring isotopes or molecular contaminants. To accomplish this, the gate time of the BNG was scanned to inject the various neighbouring isotopes in the trap. These isotopes were then identified by measuring their cyclotron frequencies and comparing them to the expected values based on the AME2020 [14] mass excess. The abundance of each isotope was also checked against the predicted ^{252}Cf fission yield. Observed contaminants not only included fission products but also molecular ions produced in the gas catcher.

To measure isomeric states, the t_{acc} was increased slowly to unambiguously observe the separation of these different states for positive identification. Most of the measurements were conducted with a $t_{acc} \sim 430$ -450ms, except for ^{114}Rh , which was measured up to 700ms to separate all three states present. Fig. 1 is a typical measurement histogram plot with all the isotopes and isomeric states for $A = 110$ identified.

Additional care was taken during measurements to minimize potential systematic effects, one of which is the non-circular beam spot path as seen on the PS-MCP. This effect is either due to a misalignment of the extraction drift tube following CPT with the magnetic field or due to the asymmetry of the magnetic field itself. Hence, for all the measurements, the reference spot and the final spot were within 10 degrees to minimize the effect of this imperfection and to minimize our dependence on the accuracy of a precise trap center measurement.

As seen in Table I, for all measurements except ^{114}Rh , for which we used nearby ^{112}Sn , we used calibrant species with the same atomic mass numbers, which effectively quench most systematic uncertainties including the ones

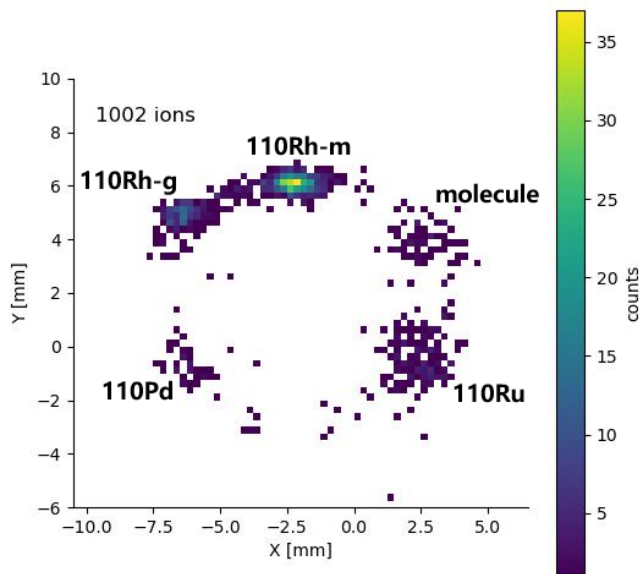


FIG. 1. A typical count histogram of the PS-MCP detector plane during the measurement of ^{110}Rh with 450.195 ms accumulation time.

due to trap misalignment, non-homogeneity of the magnetic field and electric potential imperfections.

To probe other potential systematics, we measured the cyclotron frequency of ^{133}Cs , which has a well-known mass, right after each Rh measurement. Then, using the calibrants in Table I, we calculated the mass excess of ^{133}Cs and compared it to the AME2020 [14]. As Figure 2 indicates, in every case our mass excesses are within 4keV of the AME2020. Figure 2 also gives the Birge ratio [15] of each of our ^{133}Cs determination as compared to the AME. While the Birge ratios using ^{108}Pd and ^{110}Pd as calibrants were smaller than one indicating our good agreement with the AME2020, the Birge ratio when using ^{112}Sn and ^{116}Cd as calibrants both were slightly above one. This small tension could point to either an unaccounted-for systematic effect for these specific measurements or an issue with the atomic masses of ^{112}Sn and ^{116}Cd . However, the mass excesses of both isotopes are on fairly solid footing as they come at 97% from a high-precision Q -value measurement for the double- β of these isotopes using the JYFLTRAP Penning trap [16, 17].

The tension seen for ^{112}Sn and ^{116}Cd is probably not due to the so-called mass-dependent shift in frequency ratio from the large mass difference with ^{133}Cs since no deviations are seen for ^{108}Pd and ^{110}Pd which are at a greater mass difference. Since the cause of the tension is not clear and to be conservative, we followed the procedure of the Particle Data Group [18] and inflated the uncertainty on the frequency ratio of the rhodium measurements that used ^{112}Sn and ^{116}Cd as calibrant by the corresponding Birge ratio.

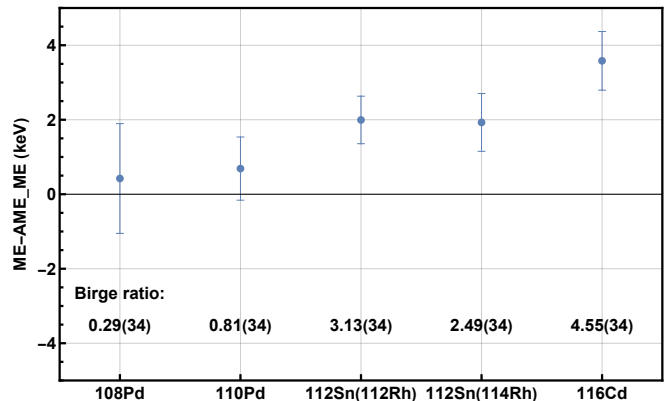


FIG. 2. ^{133}Cs mass excess deviation from the AME value with the calibrants listed in Table I. The Birge ratios of the calculated ^{133}Cs mass excess compared to the ^{133}Cs mass excess from AME2020 are also listed in the plot.

MEASUREMENT RESULTS AND DISCUSSION

The masses of the ground state and isomeric state(s) of $^{108,110,112,114,116}\text{Rh}$ were measured using 1+ charge state beams from CARIBU with the CPT during two separate campaigns. The results of these measurements are presented in Table I and shown by the black markers in Fig. 3.

The experimental mass value for $^{108,110,112,114,116}\text{Rh}$ adopted by the AME2020 mainly originates from two JYFLTRAP measurements [19, 20] and two β decay endpoint measurements of Ru β decay to Rh [21] or Rh β decay to Pd [22] together with a storage-ring measurement [23]. All experimental values adopted by the AME2020 are listed in Table II and represented by color-coded markers in Fig. 3.

AME2020 includes only the ground state and one isomeric state for $^{108,110,112,114,116}\text{Rh}$ and there are no experimental mass values of the isomeric states of $^{110,112,114,116}\text{Rh}$. In this experiment, two states were found in ^{108}Rh , ^{110}Rh and ^{116}Rh as the AME2020 predicted. However, only one state of ^{112}Rh was observed, while three states of ^{114}Rh were present.

JYFLTRAP also conducted mass measurements of $^{110,112,114,116}\text{Rh}$ recently [5] and those results are plotted for comparison in Fig. 3 by the coral-colored markers.

^{108}Rh

^{108}Rh is the only rhodium isotope we measured that has experimental values for both the ground state and the isomeric state in AME2020. Both states are based on a 2007 JYFLTRAP measurement [19] shown in blue in Fig. 3. Our ground state mass is 58(14)keV higher than the AME value while our isomeric state, with an excita-

TABLE I. Cyclotron frequency ratio and mass excess of the $^{108,110,112,114,116}\text{Rh}$ states measured by the CPT and the excitation energy calculated based on the measured mass value. The mass excess and excitation energy from the AME2020 [14] are also listed.

Nuclide	Calibration	ν_c^{ref}/ν_c	ME(keV)	ME(keV) $_{AME}$	Ex(keV)	Ex(keV) $_{AME}$
$^{108}\text{Rh}^g$	^{108}Pd	1.000045277(11)	-84973.3(16)	-85031(14)		
$^{108}\text{Rh}^m$	^{108}Pd	1.000045932(12)	-84907.5(17)	-84917(12)	65.8(23)	115(18)
$^{110}\text{Rh}^g$	^{110}Pd	1.0000549497(37)	-82705.40(72)	-82829(18)		
$^{110}\text{Rh}^m$	^{110}Pd	1.0000553408(32)	-82665.36(70)	-82610(150)#	40.0(10)	220(150)#
$^{112}\text{Rh}^m$	^{112}Sn	1.000087223(17)	-79563.0(20)	-79390(60)		340(70)
$^{114}\text{Rh}^g$	^{112}Sn	1.017997068(15)	-75661.7(17)	-75710(70)		
$^{114}\text{Rh}^m$	^{112}Sn	1.017997960(16)	-75568.8(18)	-75510(70)#	93.0(25)	200(150)#
$^{114}\text{Rh}^n$	^{112}Sn	1.017998163(16)	-75547.6(19)		114.2(25)	
$^{116}\text{Rh}^g$	^{116}Cd	1.00016653(21)	-70733(23)	-70740(70)		
$^{116}\text{Rh}^m$	^{116}Cd	1.00016766(17)	-70612(19)	-70540(170)#	121(30)	200(150)#

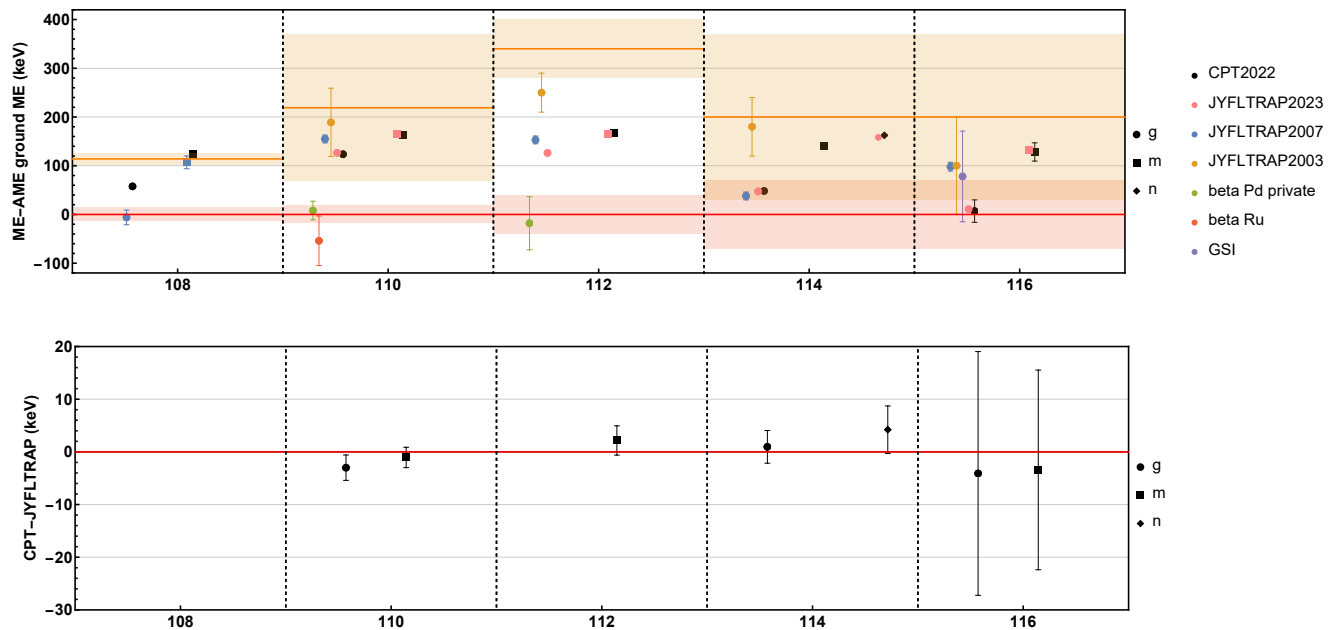


FIG. 3. Top panel: Mass excess difference between this work and the AME ground state. The red solid and dashed lines show the AME value and uncertainty range for the ground state. The orange solid and dashed lines show the AME value and uncertainty range for the isomeric state. All the experiment values adopted by the AME2020 [14] listed in Table II are shown by different colors. In addition, two JYFLTRAP measurements of ^{110}Rh are also plotted for comparison. Different states are represented by different symbols. Bottom panel: The mass difference between this work and values from the recent JYFLTRAP measurement [5] when a comparable state is present in both measurements.

tion of 65.8(23) keV, agrees with the AME2020 isomeric state mass excess. Our measurement improves the precision by an order of magnitude. The value discrepancy of the ground state mass may warrant another independent measurement.

^{110}Rh

Two states of ^{110}Rh were observed and measured in this experiment. The measured ground state is 124(18)keV higher than the current AME2020 value. The experimental values adopted for the AME2020 ground state are two beta decay endpoint measurements: one from [21] shown in green and a private communication [22] shown in red in Fig. 3. Besides the beta-endpoint

measurements, there are two Penning trap measurements by JYFLTRAP [19, 20] which are not adopted by the AME2020 and both could be a result of a mixture of the ground state and isomeric state(s) as indicated in the publication. These are also plotted in Fig. 3 for comparison. The JYFLTRAP2007 measurement [19] shown in blue lands between our ground state and isomeric state and leans closer to the latter. The JYFLTRAP2007 value would be more influenced by the isomeric state if the isomeric state was produced in greater abundance than the ground state, as was observed in this experiment. The large uncertainty in the JYFLTRAP2003 measurement [20], shown in yellow, encompasses both our ground state and isomeric state. Our ground and isomeric values agree well with the most recent JYFLTRAP measurements [5].

During the measurement, we also observed another candidate isomeric state with an excitation energy of 377.5(13) keV, which is not expected by the AME2020 or reported in [5]. However, after a complete molecule search, a stable molecule $^{82}\text{Se}^{12}\text{C}^{16}\text{O}^+$, which is only 0.018Hz away from this candidate new state in frequency was found. Although this difference is greater than the measured uncertainty of the candidate new state (0.007Hz), it corresponds to just 3 degrees on the PS-MCP detector, much smaller than the typical spot spread and below our resolution limit. Therefore, this “new candidate state” cannot be confirmed and is likely the stable $^{82}\text{Se}^{12}\text{C}^{16}\text{O}^+$ molecule instead.

^{112}Rh

Only one state of ^{112}Rh was observed in this measurement. This observed state is 167(40)keV higher than the current AME2020 ground state value but 173(60)keV lower than the theoretical isomeric state value in AME2020. The current AME value for the ^{112}Rh ground state is dominated at 66% by the beta endpoint measurements from a private communication [22] and the remaining contribution comes from the two JYFLTRAP measurements [19, 20] shown by blue and yellow in Fig. 3. The most recent JYFLTRAP measurement [5] reported both the ground state and the isomeric state but the ground state was exclusively produced by the in-trap decay of the even-even ^{112}Ru instead of being produced directly by fission [5]. The single state observed in this work has a consistent mass excess value with the isomeric state observed by JYFLTRAP. The non-observation of the ^{112}Rh ground state as produced by fission at JYFLTRAP is corroborated by our non-observation of that state. Following a further examination, the clustering algorithm identifies a hint of a possible cluster in the “tail” of the prevailing isomeric state at a similar ground state mass then [5]. It should be noted that this observation would not have been made unambiguously without prior knowledge from the JYFLTRAP measurement. Furthermore,

because the existence of that cluster was found in the analysis, the standard cyclotron frequency measurement procedure was not followed for it and as such no accurate frequency ratio corresponding to that state can be reported.

^{114}Rh

The measured ground state agrees with the current AME2020 value and the two isomeric states are also within the range of the theoretical value as reported in NUBASE2020. The literature value of the ^{114}Rh ground state in AME2020 come from the two prior JYFLTRAP measurements [19, 20]. Our ground state mass departs from JYFLTRAP2003 but is only 10(8) keV higher than the JYFLTRAP2007. Both our ground state and the isomeric state with an excitation energy of 114.2(25) keV are in agreement with the most recent JYFLTRAP measurement [5]. However, we also observed a possible additional isomeric state with a slightly lower excitation energy of 93.0(25) keV, which was not predicted in the AME2020 or reported in [5]. This observation will need to be confirmed by a decay spectroscopy measurement to unambiguously confirm its isomeric nature.

It is worth noting that unlike all the other Rh isotopes in this measurement where the production yield is predominantly from the isomeric state or the two states exhibit similar abundances, the production yield of ^{114}Rh was observed to be clearly dominated by the 1^+ ground state instead of the (7^-) isomeric state. This contradicts the expectation that the isomeric state, with its higher spin state, should be more favorably produced by fission. This inversion in production yield ratio is also reported in [5]. The inversion in the order of yield might be explained by decay loss if the half-life of the ground state is greater than the isomeric state. However only one half-life of 1.85(5) s has been observed [24]. In [25], the half-life of the high spin state has been measured to be 1.86(6) s, matching the previous value [24]. Furthermore [25] pointed out that the half-life of lower spin state 1^+ could be shorter than 1.86 s. Thus the current information of the half-life is not enough to explain the anomalous inversion of the yield. The other possibility is the inversion of the spin assignment of the ground state and isomeric state. This is discussed in more detail in the theory section.

^{116}Rh

Both our ground state and isomeric state agree with the AME2020 and NUBASE2020. The ^{116}Rh ground state AME2020 value is derived by the two JYFLTRAP measurements [19, 20] and a GSI storage-ring experiment [23]. All three measurements fall between our ground

TABLE II. Reference of the experimental values adopted by the AME2020.

Nuclide	Method	Reference
$^{108}\text{Rh}^g$	Penning Trap	U.Hager, JYFLTRAP2007[19]
$^{108}\text{Rh}^m$	Penning Trap	U.Hager, JYFLTRAP2007[19]
$^{110}\text{Rh}^g$	β -endpoint (Pd)	private communication2000[22]
	β -endpoint (Ru)	A. Jokinen1991[21]
$^{110}\text{Rh}^m$	-	-
$^{112}\text{Rh}^g$	β -endpoint (Pd)	private communication2000[22]
	Penning Trap	U.Hanger, JYFLTRAP2007[19]
	Penning Trap	V. Kolhinen, JYFLTRAP2003[20]
$^{114}\text{Rh}^g$	Penning Trap	U.Hanger, JYFLTRAP2007[19]
	Penning Trap	V. Kolhinen, JYFLTRAP2003[20]
$^{114}\text{Rh}^m$	-	-
$^{114}\text{Rh}^n$	-	-
$^{116}\text{Rh}^g$	Penning Trap	U.Hanger, JYFLTRAP2007[19]
	Penning Trap	V. Kolhinen, JYFLTRAP2003[20]
	Storage Ring	Knöbel, GSI2008[23]
$^{116}\text{Rh}^m$	-	-

state and isomeric state, which suggests that they may be the result of a mixture of two states as the publications suggested. Both our ground state and isomeric state are in close agreement with the most recent JYFLTRAP measurement in [5] as the bottom panel in Fig. 3 indicates.

Summary

This section reported new Penning trap mass measurements of the ground and isomeric states of $^{108,110,112,114,116}\text{Rh}$ that yielded consistent values with recent JYFLTRAP [5] measurements, improving the confidence on the accuracy of the mass excess of different states in these isotopes. Both groups had the same difficulty observing two states of ^{112}Rh directly from the fission beam. Additionally, both group observed the inversion in yield of the ground state and isomeric state of ^{114}Rh . In addition to the successful measurement of the ground state and one isomeric state as the AME2020 predicts, we also report the possible discovery of an additional isomeric state for ^{114}Rh .

THEORY

1^+ ground state chain

Besides all presenting one or multiple excited states, odd-odd nuclei $^{104-118}\text{Rh}$ also happen to be the longest consecutive chain of odd-odd isotopes with a spin-parity of 1^+ for their ground state [4]. To investigate this peculiar phenomena from a nuclear structure perspective, we examined the potential energy surfaces of their even-even partner ($Z - 1, N - 1$) nuclei $^{102-116}\text{Ru}$. This allows to

estimate the most typical deformation behavior for several one-particle excited states close to the Fermi surface in the neighboring odd-A nuclei of interest and extend the estimates to the odd-odd neighbors. The potential energy surface of ^{108}Ru and ^{116}Ru are plotted in Fig. 4.

Regarding the (β, γ) -plots, when only the quadrupole deformations $\{\alpha_{20}, \alpha_{22}\} \leftrightarrow \{\beta, \gamma\}$ are used (all other deformations set to zero, $\alpha_{\lambda \neq 2, \mu} = 0$), one can follow the symmetry of the shapes implying that for $\gamma \rightarrow \gamma' = \gamma + \pm k \times 90^\circ$ for $k = 1, 2, 3$) the shapes are the same the only difference being relative orientation of the body with respect to the references frame. It follows that the compared energies are equal, and one can limit the deformation space to the “triangle” $0 \leq \gamma \leq 60^\circ$, as often seen in the literature. We are performing the large scale calculations employing multidimensional deformation spaces minimizing over the selected deformations with $\lambda > 2$. Under these circumstances we should take into account various orientations of the quadrupole deformation and other multipole shapes and consider $0 \leq \gamma \leq 360^\circ$ as seen in Fig. 4. As a summary for rapid orientation: the shapes with $\gamma = \pm 60^\circ$ are oblate differing in terms of the orientation of the symmetry axis, similarly, $\gamma = 0, \pm 90^\circ$ are prolate, etc. The actual realizations of the shape and orientation will be commented below depending on the context.

The minimum potential location which is marked by the red cross indicates the most likely nuclear deformation for each given isotope. The lightest nuclei from ^{104}Ru to ^{108}Ru , Fig. 4 (top panel), are predicted to be prolate deformed. The map for ^{108}Ru is considered as representative for the other ones listed. Whereas for ^{110}Ru and ^{112}Ru predictions privilege oblate deformation. Finally, beginning with ^{114}Ru , the nuclear equilibrium deformations are predicted oblate. With such shape transition, it is then counter-intuitive to observe identical spin-parity across all isotopes.

To explain the persistence of the 1^+ presence despite the evolution of nuclear shapes, we examined the ground state spin-parity configurations of $^{104}\text{Rh} - ^{118}\text{Rh}$, to start with. To form a 1^+ configurations, the only possibility is that the protons and the neutrons carry an identical angular momenta $I_n = I_p = \frac{1}{2}$. We applied a similar approach as in [7, 26–28], i.e., following the Bohr and Mottelson maximum alignment approximation according to which the maximum alignment of nucleonic angular momentum with the symmetry axis is the privileged driving force. As an implication, one can derive the so-called titled Fermi surface algorithm, see the above references for details and illustrations.

We have calculated the particle-hole configurations for the isotopes of interest. Fig. 5 shows the so-called single particle tilted Fermi surface diagrams illustrating the proton and neutron energies as functions of the angular momentum projections on the symmetry axis, for two types of shapes. We have demonstrated that the ground-

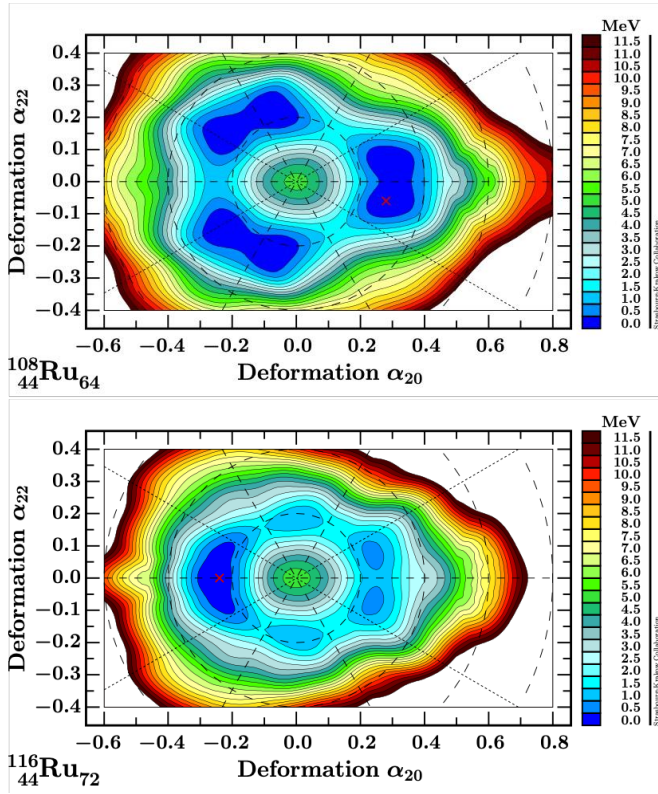


FIG. 4. Potential energies surfaces of ^{108}Ru , and ^{116}Ru with the minimum energy indicated by the red cross. ^{102}Ru , ^{104}Ru , ^{106}Ru , ^{110}Ru , and ^{114}Ru exhibit potential energy surface distribution and deformation akin to ^{108}Ru . Moreover, ^{114}Ru is similar to ^{116}Ru . Consequently, only representative plots for each group are displayed.

state energies correspond to $I^\pi = 1^+$ configurations, despite the fact that the results illustrated correspond to very different isotopes. Moreover, similar calculations for all the intermediate cases bring exactly the same results; protons keep the same configurations for all the prolate predicted nuclei with the last particle occupying the $1g_{7/2}$ with a $m_j = +1/2$ projection. For the neutrons, the last particle occupies the same $1g_{7/2}$ with a $m_j = +1/2$ projection orbital in such a way that as the neutron number increases by $\Delta N = 2$, the new particles occupy pairs of spin-up spin-down orbitals in consecutive $\pm m_j$ states. Based on these particle-hole configurations, the odd-odd isotopes $^{104-114}\text{Rh}$ are prolate and the shape becomes oblate when approaching $^{116,118}\text{Rh}$. The oblate configurations follow the same pattern as the prolate ones, with the odd proton occupying $1g_{9/2}$ -level with $m_j = 1/2$ projection, whereas the neutrons occupying their levels pairwise with the odd one at $g_{7/2}$ -level with $m_j = 1/2$. Such observation is consistent with the results presented in the potential energy surfaces and would provide, for the first time, an explanation for steady 1^+ despite a rapid shape transition.

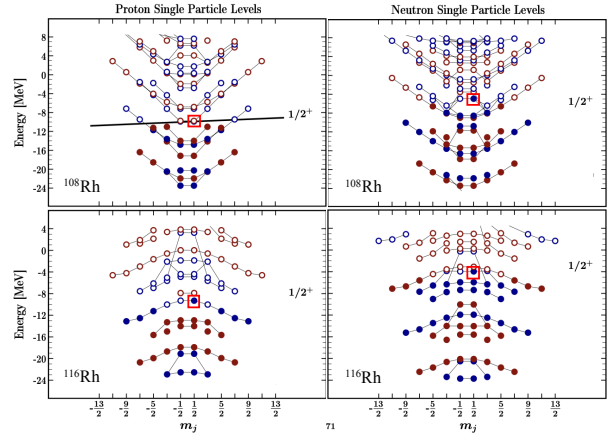


FIG. 5. Single particle energy levels as functions of the nucleonic angular momentum projections on the symmetry axis – diagrams often referred to as the so-called “umbrella plots”. Blue (red) circles stand for positive (negative) parity levels. Full circles stand for occupied state and open circles mean unoccupied states. Black thin connecting lines between bullets have no physical meaning, they are meant to connect same nl_j -levels. Unpaired nucleons are indicated by the red square. According to Bohr and Mottelson maximum alignment hypothesis the total spins of the discussed configurations are approximated by the corresponding projections on the symmetry axis constructed as algebraic sums of contributions from the particle-hole configurations.

TABLE III. Deformation parameters ^{a)} used in the multi-quasiparticle blocking calculations.

Nuclide	prolate		oblate			
	β_2	β_4	β_6	β_2	β_4	β_6
^{108}Rh	+0.250	+0.011	-0.001	-0.248	-0.034	+0.002
^{110}Rh	+0.260	+0.005	-0.001	-0.248	-0.034	+0.002
^{112}Rh	+0.265	+0.005	-0.001	-0.248	-0.044	+0.014
^{114}Rh	+0.265	+0.005	-0.001	-0.258	-0.053	+0.018
^{116}Rh	+0.260	+0.005	-0.001	-0.258	-0.064	+0.012

^{a)} Values for ^{108}Rh and $^{110,112,114,116}\text{Rh}$ are from Ref. [29].

Multi-quasiparticle blocking calculations

In order to predict the structure of low-lying states in the odd-odd Rh nuclei, multi-quasiparticle blocking calculations were carried out for both prolate and oblate deformations by assuming axial symmetry. The energies of single-particle states were taken from the Woods-Saxon potential with the “universal” parameterization [30] and the adopted deformation parameters β_2 , β_4 and β_6 are summarized in Table III. The pairing correlations were treated using the Lipkin-Nogami prescription [31] with fixed strengths of $G_\pi = 24.0/A$ MeV (protons) and $G_\nu = 17.8/A$ MeV (neutrons) and they included the effect of blocking. Calculations did not include the effect of the residual proton-neutron interactions, and therefore,

it was not possible to predict the excitation energies of the predicted states. Instead, the so-called Gallagher-Moszkowski rule [32] was applied to establish the ordering of the $|\Omega_p - \Omega_n|$ and $\Omega_p + \Omega_n$ states within a given $\Omega_p \otimes \Omega_n$ configuration, where Ω is the projection of the angular momentum on the symmetry axis. The predicted most-likely configurations for the ground and isomeric states in the odd-odd Rh nuclei are given in Table IV. Also in Table IV predictions based on the known experimental states in neighboring odd-Z, even-N Rh and even-Z, odd-N Ru nuclei [4, 33] are given under the empirical column. The systematic of experimental values [4] show that all odd-Z, even-N $^{107-115}\text{Rh}$ nuclei have the $I^\pi=7/2^+$ ground state, associated with prolate shape and the $\pi 7/2[413]$ Nilsson orbital. At the same time, the experimental ground state of the odd-N, even-Z $^{107,109,111}\text{Ru}$ (N=63-67) nuclei is assigned to be $5/2^+$, which correspond to a $\nu 5/2[413]$ Nilsson orbital. Thus, the lowest-energy configuration in the odd-odd $^{108,110,112}\text{Rh}$ (N=63-67) nuclei is expected to be $\pi 7/2[413] \otimes \nu 5/2[413]$ and in accordance with the Gallagher-Moszkowski rule [32], $I^\pi=1^+$ for the ground states and $I^\pi=6^+$ for the isomers. Such assignments are in a relatively good agreement with the predictions from the multi-quasiparticle blocking calculations for prolate shapes. This is consistent with the calculation results presented in the previous section. The structure of the heavier $^{113,115}\text{Ru}$ (N=69,71) is not well established and there are evidences for competing prolate and oblate configurations, also as evidenced by the calculation from the previous section. Recently, the $\nu 1/2[411]$ Nilsson orbital was proposed for the ground state of these nuclei, while the isomer was associated with the $\nu 7/2[523]$ orbital [34, 35]. The expected configurations for the odd-odd $^{114,116}\text{Rh}$ (N=69,71) nuclei are given in Table IV. Once again, following the Gallagher-Moszkowski rule [32] and assuming a $\pi 7/2[413] \otimes \nu 1/2[411]$ configuration for the ground state, a $I^\pi=3^+$ is expected for both $^{114,116}\text{Rh}$. This value differs from the observed $I^\pi=1^+$ [4]. The isomeric state on the other hand appears to be in a $\pi 7/2[413] \otimes \nu 7/2[523]$ configuration yielding a $I^\pi=7^-$. The isomeric state value of 7^- do agree with the experimental value for ^{114}Rh but not with the 6^- value for ^{116}Rh . Furthermore, these empirical configurations do not yield an inversion in the spin-parity of the ground and isomeric states. However, the multi-quasiparticle blocking calculations predictions for both the oblate and prolate shapes yield a higher spin for the ground state of $^{114,116}\text{Rh}$ than their isomeric states. This contradicts the empirical configuration while agreeing with the observed yield ratio for ^{114}Rh . Hence, there is a strong impetus for a direct spin determination using laser spectroscopy on neutron-rich, odd-odd Rh isotopes, in particular ^{114}Rh .

CONCLUSION

The ground state and isomeric state(s) of $^{108,110,112,114,116}\text{Rh}$ were identified and their masses were measured with high precision using the Canadian Penning Trap and the CARIBU facility. The obtained ground state mass excesses and isomeric state excitation energies are consistent with recent measurements from the JYFLTRAP Penning trap. Furthermore, a possible second isomeric state has also been found for ^{114}Rh .

The measured isotopes also happen to be part of the longest chain of odd-odd isotopes carrying identical spin-parity (1^+) across the whole nuclear chart amid known changes in shape. Detailed nuclear structure calculations were performed to investigate this peculiarity. This was accomplished using potential energy surface calculations that showed the observed change of deformation along this odd-odd isotopic line. Furthermore, particle-hole configurations were calculated to explain this deformation without altering the spin-parity finally shedding light on this peculiar phenomena.

In addition, multiquasiparticle blocking calculations were conducted to explore alternative spin-parity assignments different from the literature value, as a potential explanation for the anomalous yield of ^{114}Rh . We found a different empirical ground state of $I^+ = 3^+$ that differs from the experimental evaluation [4] while the empirical isomeric state yield a consistent value of $I^+ = 7^-$. However multiquasiparticle blocking calculations assuming either prolate or oblate shape results in a spin inversion with the ground state having a higher spin than the isomeric state, which is consistent with what we have observed experimentally.

Hence, there is a strong need for a direct measurement of the nuclear spin of ^{114}Rh using laser spectroscopy to shed light on the situation. Such measurement on the other odd-odd isotopes in the $^{104-118}\text{Rh}$ chain is also warranted to confirm the $I = 1$ spin assignment of their ground states.

Finally, given only one half-life of the two isomeric states of ^{114}Rh has been reported in literature, a new half-life measurement would be helpful to clarify the inversion of the fission yield and spin-parity assignment.

ACKNOWLEDGMENTS

This work is supported in part by the National Science Foundation under Grant No. PHY-2310059; by the University of Notre Dame; and with resources of ANL's ATLAS facility, an Office of Science User Facility; by the U.S. Department of Energy, Office of Nuclear Physics, under Contract No. DE-AC02-06CH11357; by NSERC (Canada), Application No. SAPPJ-2018-00028.

TABLE IV. Predicted configuration for the ground states and the isomers in the odd-odd $^{108,110,112,114,116}\text{Rh}$ nuclei.

Nuclide	I^π	prolate Configuration	I^π	oblate Configuration	I^π	empirical Configuration
^{108}Rh	2^+	$\pi 1/2[301] \otimes \nu 5/2[532]$	1^+	$\pi 3/2[411] \otimes \nu 5/2[413]$	1^+	$\pi 7/2[413] \otimes \nu 5/2[413]$
	6^-	$\pi 7/2[413] \otimes \nu 5/2[532]$				
^{108m}Rh	1^+	$\pi 7/2[413] \otimes \nu 5/2[413]$	4^+	$\pi 3/2[411] \otimes \nu 5/2[413]$	6^+	$\pi 7/2[413] \otimes \nu 5/2[413]$
	1^-	$\pi 7/2[413] \otimes \nu 5/2[532]$			6^-	$\pi 7/2[413] \otimes \nu 5/2[532]$
	6^+	$\pi 7/2[413] \otimes \nu 5/2[413]$				
^{110}Rh	1^+	$\pi 7/2[413] \otimes \nu 5/2[413]$	6^-	$\pi 3/2[411] \otimes \nu 9/2[514]$	1^+	$\pi 7/2[413] \otimes \nu 5/2[413]$
	6^-	$\pi 7/2[413] \otimes \nu 5/2[532]$				
^{110m}Rh	6^+	$\pi 7/2[413] \otimes \nu 5/2[413]$	1^+	$\pi 3/2[411] \otimes \nu 1/2[411]$	6^+	$\pi 7/2[413] \otimes \nu 5/2[413]$
	1^-	$\pi 7/2[413] \otimes \nu 5/2[532]$	3^-	$\pi 3/2[411] \otimes \nu 9/2[514]$	6^-	$\pi 7/2[413] \otimes \nu 5/2[532]$
^{112}Rh	3^+	$\pi 7/2[413] \otimes \nu 1/2[411]$	1^+	$\pi 3/2[411] \otimes \nu 1/2[411]$	1^+	$\pi 7/2[413] \otimes \nu 5/2[413]$
					3^+	$\pi 7/2[413] \otimes \nu 1/2[411]$
^{112m}Rh	6^-	$\pi 7/2[413] \otimes \nu 5/2[532]$	6^-	$\pi 3/2[411] \otimes \nu 9/2[514]$	6^+	$\pi 7/2[413] \otimes \nu 5/2[413]$
^{114}Rh	6^+	$\pi 7/2[413] \otimes \nu 5/2[402]$	5^-	$\pi 3/2[411] \otimes \nu 7/2[523]$	3^+	$\pi 7/2[413] \otimes \nu 1/2[411]$
	7^-	$\pi 7/2[413] \otimes \nu 7/2[523]$				
^{114m}Rh	1^+	$\pi 7/2[413] \otimes \nu 5/2[402]$	2^-	$\pi 3/2[411] \otimes \nu 7/2[523]$	7^-	$\pi 7/2[413] \otimes \nu 7/2[523]$
	$0^-, 1^-$	$\pi 7/2[413] \otimes \nu 7/2[523]$				
^{116}Rh	7^-	$\pi 7/2[413] \otimes \nu 7/2[523]$	4^-	$\pi 3/2[411] \otimes \nu 5/2[512]$	3^+	$\pi 7/2[413] \otimes \nu 1/2[411]$
	6^+	$\pi 7/2[413] \otimes \nu 5/2[402]$				
^{116m}Rh	$0^-, 1^-$	$\pi 7/2[413] \otimes \nu 7/2[523]$	1^-	$\pi 3/2[411] \otimes \nu 5/2[512]$	7^-	$\pi 7/2[413] \otimes \nu 7/2[523]$
	1^+	$\pi 7/2[413] \otimes \nu 5/2[402]$				

- [1] P. E. Garrett, M. Zielinska, and E. Clement, An experimental view on shape coexistence in nuclei, *Progress in Particle and Nuclear Physics* **124**, 103931 (2022).
- [2] R. Orford, F. G. Kondev, G. Savard, J. A. Clark, W. S. Porter, D. Ray, F. Buchinger, M. T. Burkey, D. A. Gorelov, D. J. Hartley, J. W. Klimes, K. S. Sharma, A. A. Valverde, and X. L. Yan, Spin-trap isomers in deformed, odd-odd nuclei in the light rare-earth region near $n = 98$, *Phys. Rev. C* **102**, 011303 (2020).
- [3] S. Eliseev, K. Blaum, M. Block, C. Droese, M. Goncharov, E. Minaya Ramirez, D. A. Nesterenko, Y. N. Novikov, and L. Schweikhard, Phase-imaging ion-cyclotron-resonance measurements for short-lived nuclides, *Phys. Rev. Lett.* **110**, 082501 (2013).
- [4] F.G.Kondev, M.Wang, W.J.Huang, S.Naimi, and G.Audi, *Chin.Phys.C* **45**, 030001 (2021).
- [5] M. Hukkanen, W. Ryssens, P. Ascher, M. Bender, T. Eronen, S. Grévy, A. Kankainen, M. Stryjczyk, L. Al Ayoubi, S. Ayet, O. Beliuskina, C. Delafosse, W. Gins, M. Gerbaux, A. Husson, A. Jokinen, D. A. Nesterenko, I. Pohjalainen, M. Reponen, S. Rinta-Antila, A. de Roubin, and A. P. Weaver, Odd-odd neutron-rich rhodium isotopes studied with the double penning trap jyfltrap, *Phys. Rev. C* **107**, 014306 (2023).
- [6] R. D. Woods and D. S. Saxon, Diffuse surface optical model for nucleon-nuclei scattering, *Phys. Rev.* **95**, 577 (1954).

- [7] W. S. Porter, B. Ashrafkhani, J. Bergmann, C. Brown, T. Brunner, J. D. Cardona, D. Curien, I. Dedes, T. Dickel, J. Dudek, E. Dunling, G. Gwinner, Z. Hockenbery, J. D. Holt, C. Hornung, C. Izzo, A. Jacobs, A. Javaji, B. Kootte, G. Kripkó-Koncz, E. M. Lykiardopoulou, T. Miyagi, I. Mukul, T. Murböck, W. R. Plaß, M. P. Reiter, J. Ringuette, C. Scheidenberger, R. Silwal, C. Walls, H. L. Wang, Y. Wang, J. Yang, J. Dilling, and A. A. Kwiatkowski, Mapping the $n = 40$ island of inversion: Precision mass measurements of neutron-rich fission isotopes, *Phys. Rev. C* **105**, L041301 (2022).
- [8] G. Savard, S. Baker, C. Davids, A. Levand, E. Moore, R. Pardo, R. Vondrasek, B. Zabransky, and G. Zinkann, Radioactive beams from gas catchers: The caribu facility, *Nuclear Instruments and Methods in Physics Research Section B: Beam Interactions with Materials and Atoms* **266**, 4086 (2008), proceedings of the XVth International Conference on Electromagnetic Isotope Separators and Techniques Related to their Applications.
- [9] C. N. Davids and D. Peterson, A compact high-resolution isobar separator for the caribu project, *Nuclear Instruments and Methods in Physics Research Section B: Beam Interactions with Materials and Atoms* **266**, 4449 (2008), proceedings of the XVth International Conference on Electromagnetic Isotope Separators and Techniques Related to their Applications.
- [10] T. Y. Hirsh, N. Paul, M. Burkey, A. Aprahamian, F. Buchinger, S. Caldwell, J. A. Clark, A. F. Levand, L. L. Ying, S. T. Marley, G. E. Morgan, A. Nystrom, R. Orford, A. P. Galvan, J. Rohrer, G. Savard, K. S.

- Sharma, and K. Siegl, First operation and mass separation with the caribu mr-tof, *Nuclear Instruments and Methods in Physics Research Section B: Beam Interactions with Materials and Atoms* **376**, 229 (2016), proceedings of the XVIIth International Conference on Electromagnetic Isotope Separators and Related Topics (EMIS2015), Grand Rapids, MI, U.S.A., 11-15 May 2015.
- [11] M. König, G. Bollen, H.-J. Kluge, T. Otto, and J. Szerypo, Quadrupole excitation of stored ion motion at the true cyclotron frequency, *International Journal of Mass Spectrometry and Ion Processes* **142**, 95 (1995).
- [12] G. Bollen, R. B. Moore, G. Savard, and H. Stolzenberg, The accuracy of heavy ion mass measurements using time of flight-ion cyclotron resonance in a Penning trap, *J. Appl. Phys.* **68**, 4355 (1990).
- [13] R. Orford, J. Clark, G. Savard, A. Aprahamian, F. Buchinger, M. Burkey, D. Gorelov, J. Klimes, G. Morgan, A. Nystrom, W. Porter, D. Ray, and K. Sharma, Improving the measurement sensitivity of the canadian penning trap mass spectrometer through pi-icr, *Nuclear Instruments and Methods in Physics Research Section B: Beam Interactions with Materials and Atoms* **463**, 491 (2020).
- [14] M. Wang, W. Huang, F. Kondev, G. Audi, and S. Naimi, The ame 2020 atomic mass evaluation (ii). tables, graphs and references*, *Chinese Physics C* **45**, 030003 (2021).
- [15] R. T. Birge, The calculation of errors by the method of least squares, *Phys. Rev.* **40**, 207 (1932).
- [16] S. Rahaman, V.-V. Elomaa, T. Eronen, J. Hakala, A. Jokinen, A. Kankainen, J. Rissanen, J. Suhonen, C. Weber, and J. Äystö, Accurate q value for the ^{112}Sn double- β decay and its implication for the search of the neutrino mass, *Phys. Rev. Lett.* **103**, 042501 (2009).
- [17] S. Rahaman, V.-V. Elomaa, T. Eronen, J. Hakala, A. Jokinen, A. Kankainen, J. Rissanen, J. Suhonen, C. Weber, and J. Äystö, Double-beta decay q values of ^{116}Cd and ^{130}Te , *Physics Letters B* **703**, 412 (2011).
- [18] J. Beringer *et al.* (Particle Data Group), Review of particle physics*, *Phys. Rev. D* **86**, 010001 (2012).
- [19] U. Hager, V.-V. Elomaa, T. Eronen, J. Hakala, A. Jokinen, A. Kankainen, S. Rahaman, S. Rinta-Antila, A. Saastamoinen, T. Sonoda, and J. Äystö, Precision mass measurements of neutron-rich ^{112}Te , ^{114}Ru , ^{116}Rh , and ^{118}Pd isotopes, *Phys. Rev. C* **75**, 064302 (2007).
- [20] V. Kolhinen, Phd thesis, University of Jyväskylä (2003).
- [21] A. Jokinen, J. Äystö, P. Dendooven, K. Eskola, Z. Janas, P. Jauho, M. Leino, J. Parmonen, H. Penttilä, K. Rykaczewski, and P. Taskinen, Spin-flip beta-decay of even-even deformed-nuclei ^{110}Ru and ^{112}Ru , *Zeitschrift für Physik. A, Hadrons and nuclei* **340**, 21 (1991).
- [22] K.-L. Kratz and B. Pfeiffer, private communication (2000).
- [23] Knöbel, Phd thesis, GSI (2008).
- [24] J. Äystö, C. Davids, J. Hattula, J. Honkanen, K. Honkanen, P. Jauho, R. Julin, S. Juutinen, J. Kumpulainen, T. Lönnroth, A. Pakkanen, A. Passoja, H. Penttilä, P. Taskinen, E. Verho, A. Virtanen, and M. Yoshii, Levels in ^{110}Pd , ^{112}Pd , ^{114}Pd and ^{116}Pd from the beta decays of the on-line mass separated ^{112}Rh isotopes, *Nuclear Physics A* **480**, 104 (1988).
- [25] G. Lhersonneau, Y. Wang, R. Capote, J. Suhonen, P. Dendooven, J. Huikari, K. Peräjärvi, and J. C. Wang, Decay of ^{114}Rh to ^{114}Pd , *Phys. Rev. C* **67**, 024303 (2003).
- [26] M. J. A. de Voigt, J. Dudek, and Z. Szymański, High-spin phenomena in atomic nuclei, *Rev. Mod. Phys.* **55**, 949 (1983).
- [27] C. Hornung, D. Amanbayev, I. Dedes, G. Kripko-Koncz, I. Miskun, N. Shimizu, S. Ayet San Andres, J. Bergmann, T. Dickel, J. Dudek, J. Ebert, H. Geissel, M. Gorska, H. Grawe, F. Greiner, E. Haettner, T. Otsuka, W. R. Plass, S. Purushothaman, A.-K. Rink, C. Scheidenberger, H. Weick, S. Bagchi, A. Blazhev, O. Charviakova, D. Curien, A. Finlay, S. Kaur, W. Lippert, J.-H. Otto, Z. Patyk, S. Pietri, Y. K. Tanaka, Y. Tsunoda, and J. S. Winfield, Isomer studies in the vicinity of the doubly-magic nucleus ^{100}Sn : Observation of a new low-lying isomeric state in ^{97}Ag , *Physics Letters B* **802**, 135200 (2020).
- [28] S. Beck, B. Kootte, I. Dedes, T. Dickel, A. A. Kwiatkowski, E. M. Lykiardopoulou, W. R. Plaß, M. P. Reiter, C. Andreoiu, J. Bergmann, T. Brunner, D. Curien, J. Dilling, J. Dudek, E. Dunling, J. Flowerdew, A. Gaamouci, L. Graham, G. Gwinner, A. Jacobs, R. Klawitter, Y. Lan, E. Leistenschneider, N. Minkov, V. Monier, I. Mukul, S. F. Paul, C. Scheidenberger, R. I. Thompson, J. L. Tracy, M. Vansteenkiste, H.-L. Wang, M. E. Wieser, C. Will, and J. Yang, Mass measurements of neutron-deficient ^{112}Yb isotopes and nuclear structure at the extreme proton-rich side of the $n = 82$ shell, *Phys. Rev. Lett.* **127**, 112501 (2021).
- [29] P. Moller, A. Sierk, T. Ichikawa, and H. Sagawa, Decay of ^{114}Rh to ^{114}Pd , *At.Data Nucl.Data Tables* **109-110**, 1 (2016).
- [30] S. Cwiok, J. Dudek, W. Nazarewicz, J. Skalski, and T. Werner, *Comput. Phys. Commun.* **46**, 379 (1987).
- [31] W. Nazarewicz, J. Dudek, R. Bengtsson, T. Bengtsson, and I. Ragnarsson, *Nucl. Phys. A* **435**, 397 (1985).
- [32] C.J.Gallagher and S.A.Moszkowski, *Phys. Rev.* **111**, 1282 (1958).
- [33] From ENSDF database as of April 9 2024. Version available at <http://www.nndc.bnl.gov>.
- [34] J.Kurpeta, C. W.Urban, A.Plochocki, S.G.Rohozinski, T.Rzaca-Urban, T.Morek, L.Prochniak, K.Starosta, J.Aysto, H.Penttila, J.L.Durell, A.G.Smith, G.Lhersonneau, and I.Ahmad, Low-spin structure of ^{113}Ru and ^{113}Rh , *Eur.Phys.J. A* **33**, 307 (2007).
- [35] J.Kurpeta, J.Rissanen, A.Plochocki, W.Urban, V.-V.Elomaa, T.Eronen, J.Hakala, A.Jokinen, A.Kankainen, P.Karvonen, T.Malkiewicz, I.D.Moore, H.Penttila, A.Saastamoinen, G.S.Simpson, C.Weber, and J.Aysto, New isomer and decay half-life of ^{115}Ru , *Phys.Rev. C* **82**, 064318 (2010).
- [36] S. Eliseev, K. Blaum, M. Block, A. Dörr, C. Droese, T. Eronen, M. Goncharov, M. Höcker, J. Ketter, E. M. Ramirez, D. A. Nesterenko, Y. N. Novikov, and L. Schweikhard, *Applied physics. B, Lasers and optics* **114**, 107 (2014).
- [37] M. Hukkanen, W. Ryssens, P. Ascher, M. Bender, T. Eronen, S. Grévy, A. Kankainen, M. Stryczyk, L. A. Ayoubi, S. Ayet, O. Beliuskina, C. Delafosse, W. Gins, M. Gerbaux, A. Husson, A. Jokinen, D. A. Nesterenko, I. Pohjalainen, M. Reponen, S. Rinta-Antila, A. de Roubin, and A. P. Weaver, *Odd-odd neutron-rich Rhodium isotopes studied with the double Penning trap JYFLTRAP*, *arXiv* (2022).
- [38] L. H. Frey, W. Even, D. J. Whalen, C. L. Fryer, A. L. Hungerford, C. J. Fontes, and J. Colgan, *The los alamos*

supernova light-curve project: Computational methods,

[The Astrophysical Journal Supplement Series 204, 16 \(2013\).](#)